SUPPORTING INFORMATION

Molecular Characterization of Organosulfates in Organic Aerosols from Shanghai and Los Angeles Urban Areas by Nanospray-Desorption Electrospray Ionization High-Resolution Mass Spectrometry

Shikang Tao[a]†, Xiaohui Lu[a]†, Nicole Levac[b], Adam P. Bateman[b], Tran B. Nguyen[b], David L. Bones[b], Sergey A. Nizkorodov[b], Julia Laskin[c], Alexander Laskin[d,]*, Xin Yang[a,e,]*

[a] *Shanghai Key Laboratory of Atmospheric Particle Pollution and Prevention, Department of Environmental Science and Engineering, Fudan University, Shanghai 200433, China*
[b] *Department of Chemistry, University of California, Irvine, CA, 92697, USA*
[c] *Physical Sciences Division,* [d] *William R. Wiley Environmental Molecular Sciences Laboratory, Pacific Northwest National Laboratory, Richland, WA, 99354, USA*
[e] *Fudan Tyndall Centre, Fudan University, Shanghai 200433, China*
† *These two authors contributed equally to the work.*

*corresponding authors:

email: alexander.laskin@pnl.gov, telephone: 509-371-6129, fax: 509-371-6139

email: yangxin@fudan.edu.cn, telephone: 86-21-5665272, fax: 86-21-55662020

Table of Contents

Part S1. Experimental Section

S1.1 Collection of Aerosol Samples

Aerosol samples collected during long-term studies in urban areas of Los Angeles (LA) and Shanghai (SH) were chosen for in-depth molecular characterization using nano-DESI HR-MS analysis. Samples from LA were collected at an urban site in Pasadena during CalNex field study (May 15th ~ June 14th, 2010).[1] Real-time records of an aerosol mass spectrometer (AMS) [2] were used to select a few of the samples during the episodes of highest (>10 μg m^{-3}) organic aerosol concentration in ambient air. Out of them, the abundant MS peaks of organosulfates were observed in the sample collected at noon ~ 6pm (local time) on May 19th 2010. Samples from SH were collected on the roof of building of the department of Environmental Science & Engineering, Fudan University, which is near a commercial center of urban Shanghai. The air pollution data (Figure S1) show that the carbonaceous compounds in atmospheric aerosols on April 15th 2011 were of highest concentration during April 10th ~ April 20th 2011. Hence, the MS we discuss in this paper are for the sample from SH collected at 6am ~ 6pm (local time) on April 15th 2011.

Corresponding backward trajectories of air mass arriving to the sampling sites were calculated using HYSPLIT model and are shown in Figure S2. In both cases, sampled particulates corresponded to the low-wind continental air masses that stayed within the urban surface boundary layer for 6-12 hours prior to the sampling. In LA, size-segregated aerosol samples were collected on Teflon substrates using a 10-stage micro-orifice uniform deposition impactor (MOUDI) (model 110R, MSP, Inc). During the sampling time average temperature and humidity were 19°C and 70% RH, respectively. In SH, size-segregated aerosol samples were collected on aluminum foil substrates using an Anderson 8-stage non-viable cascade impactor (Series 20-800, Thermo Fisher Scientific). The average temperature and humidity were 23°C and 71% RH, respectively. To facilitate comparison between aerosol samples of similar particle sizes, we use the SH sample collected on the 8th stage of the Anderson impactor and the LA sample collected on the 7th stage of MOUDI. Particles collected on these two stages showed highest mass loadings and their corresponding aerodynamic sizes are 0.4–0.7μm for SH sample and 0.32–0.56μm for LA sample.

S1.2 Nano-DESI Mass Spectrometry

Aerosol samples deposited on substrates were analyzed using an LTQ-Orbitrap High Resolution Mass Spectrometer (Thermo Electron Bremen, Germany) equipped with a custom-built nano-DESI source.[3,4] The analysis was performed about 2 months later after the sampling, for either LA sample or SH sample. The nano-DESI probe is assembled from two fused silica capillaries (193μm o.d., 50μm i.d.). One capillary is used to supply the desired working solvent at a flow rate of 0.3–1.0 μL/min. The flow rate is optimized to maintain a liquid bridge between the two capillaries. When the liquid bridge is brought in contact with the sample, analyte molecules are dissolved and transported with the solvent through a self-aspirating capillary that generates ions by nanoelectrospray at the MS inlet. The solvents used in this work were AcN/H_2O (v/v=1/1) and AcN/Tol (v/v=7/3). The mass spectrometer was operated in both positive (+) and negative (–) ion modes with spray voltage of 3.5–4.2kV and mass resolving power of m/Δm ~ 100,000 at *m/z* 400. The background mass spectra were acquired by positioning the nano-DESI probe on the substrate outside of the visually identified aerosol deposition area, while the sample spectra were acquired by positioning the probe within the aerosol containing area.[3]

S1.3 Data Analysis and Processing

Detected peaks in the *m/z* range of 150–500 were analyzed using a suite of data analysis tools developed at PNNL. Peaks with the S/N ratio of 3 and higher were extracted from raw spectra using Decon2LS (http://omics.pnl.gov/software/decontools-decon2ls). Removal of the background peaks and all ^{13}C-containing peaks was performed using an Excel macro with a tolerance of 0.001 *m/z* units (peaks in different spectra were considered the same if they were separated by less than the tolerance). The remaining peaks were assigned with elemental formulas using the Molecular Formula Calculator (http://www.magnet.fsu.edu/usershub/scientificdivisions/icr/icr_software.html). The formula search was constrained using the following limits on elemental composition: $C_{1-40}H_{2-80}O_{0-40}N_{0-3}S_{0-2}Na_{0-1}^{+}$ in positive mode, and $C_{1-40}H_{2-80}O_{0-40}N_{0-3}S_{0-2}^{-}$ in negative mode.

Assignments were aided by a second-order Kendrick mass defect analysis using CH_2 and H_2 as bases.[5] The observed molecular formulas were assumed to correspond to either protonated or sodiated molecules in the positive mode, and to deprotonated molecules in the negative mode. The ionic formulas were subsequently converted into neutral formulas, $C_cH_hO_oN_nS_s$. In order to eliminate compounds not likely to be observed in nature, all neutral formulas $C_cH_hO_oN_nS_s$ were further filtered using the following rules [6,7]: the H/C and O/C ratios were limited to 0.3–2.25 and 0–1.2 respectively (using (O–3)/C instead of O/C if the formula contains S or N and is in the negative mode); the N/C and S/C ratios were limited to 0–1.3 and 0–0.8 for positive mode and 0–0.5 and 0–0.2 for negative mode; and DBE/C ratios were limited to 0–1. Here, the DBE indicates double bond equivalent, calculated by Eq S1.

$$DBE = (2c+2+n-h)/2 \qquad \text{(Eq S1)}$$

It should be noted that in the calculation of DBE in this paper we have assumed a valence of 3 for nitrogen and a valence of 2 for sulfur. This approach underestimates the true value of DBE in organosulfates and organonitrates. Therefore, reported DBE values are considered as the low-limit.

Kendrick diagrams were not only used to help rule out ambiguous assignments in the formula searching work, but also to help compare the CHOS species in different samples. In Kendrick diagrams, the experimentally measured *m/z* is normalized to the nominal mass of a selected chemical group (e.g., CH_2, O, CH_2O).[8] For example, in a CH_2-Kendrick diagram the Kendrick mass (KM_{CH2}) is calculated by renormalizing the IUPAC mass scale to the exact mass of the $^{12}CH_2$ group using Eq 2 and the Kendrick mass defect (KMD_{CH2}) is calculated as the difference between the nominal value of KM_{CH2} (14 Da) and KM_{CH2} using Eq 3. In this representation, homologous CH_2-series fall on the horizontal lines and are clearly distinguishable in the diagram with KMD_{CH2} plotted against KM_{CH2}.

$$KM_{CH2} = \text{Observed Mass} \times \left(\frac{14.00000}{14.01565}\right) \qquad \text{(Eq S2)}$$

$$KMD_{CH2} = \text{Nominal Mass} - KM_{CH2} \qquad \text{(Eq S3)}$$

S1.4 Unassigned peaks

The number of unassigned peaks in SH sample is similar to that in LA sample.(Table 1 in the manuscript) For either SH sample or LA sample, the total number of unassigned peaks is higher in AcN/H_2O(–) MS than in the other spectra, indicating water-soluble polar organic compounds. The unassigned compounds are likely compounds with elemental composition outside of the limits applied for the formula search. These may also include molecules containing additional elements not included in the search, and molecules with higher number of S and N atoms.

Part S2. Detailed Analysis of CHO and N-OC species

S2.1 CHO species

On average, for CHO detected in either mode, the fraction is considerably smaller in SH sample than in LA sample. This could results from the heavier aerosol mass loading for SH sample. (The daily average mass concentrations of $PM_{2.5}$ in Shanghai and Los Angeles on the sampling days were 150 and <10 μg/m^3, respectively.) The heavily loaded inorganic species in SH sample may render the ionization of oxygenated hydrocarbons suppressed. Another plausible reason is that heavy pollution in Shanghai leads to much higher concentration of sulfuric acid, facilitating the conversion of organic compounds to organosulfates, which, in turn, represent the most abundant group of peaks in SH sample. Characteristic H/C and O/C ratios of CHO species are illustrated by the Van Krevelen (VK) diagrams[9] of Figure S5. CHO detected in the negative mode have higher O/C ratios than those in the positive mode, possibly because of favored deprotonation of oxygen-rich carboxyl groups in CHO species that result in their enhanced detection in the negative modes. The O/C ratio of CHO compounds in SH sample, is either lower than 0.25 or greater than 0.55 while large amounts of CHO with O/C ratios from 0.25 to 0.55 are present in LA sample. This comparison shows that CHO observed in SH sample are characterized by either very low or very high degree of oxidization, likely reflecting the contribution of both primary and secondary organics to the particle composition. These two types of CHO in SH sample are not the majority of CHO in

LA sample.

S2.2 N-OC species

In both SH and LA samples, N-OC species are dominated by CHON and CHN groups in the positive mode, and by CHONS group in the negative mode. Figure S6 shows the VK diagrams with the O/N ratio against the O/C ratio for N-OC species. In the LA sample, the majority of N-OC have high O/N ratios and only one nitrogen atom. It follows that N-OC species in LA sample could include both organonitrates and amines/imines. According to the reported studies of SOA aging, the reduced nitrogen is usually added to the organic compounds via imine formation. [10] The mechanisms of these reactions suggest that the mass difference between N-OC species and their plausible CHO precursors would have characteristic values that can be used to relate potential precursor-product pairs.[10,11] Using this methodology, we compared CHON and CHN species versus CHO species observed in LA sample (positive mode) and confirmed that more than 60% of CHON and CHN species have precursor/product pairs consistent with imine formation reactions (Figure S7). Distribution of N/C versus O/C ratios in the space of VK diagrams is also similar to that of the reduced nitrogen organics reported previously by O'Brien et al.[11] All these observations suggest that CHON and CHN species in LA sample may include a large number of reduced nitrogen compounds

Compared with a large number and strong intensity of CHON and CHN peaks observed in LA sample, only 30 peaks assigned to CHON or CHN were observed in SH sample. The reduced nitrogen species in organic aerosols of SH sample were also in the minority. In view of the higher NOx concentration in Shanghai, one would expect organonitrates as a major constituent. However, organonitrates of CHON appear to be minor. In addition to the similar reasons for the poor observation of CHO, another possible reason for the paucity of observation of organonitrates of CHON is that organonitrates, usually formed in the gas phase, require additional functionalization to efficiently partition to the particle phase.[12,13] Organonitrates without sulfate groups are less stable with respect to nucleophilic substitution reactions with water or sulfate.[13,14] Indeed, almost all the N-OC with high O/N ratio were

assigned to CHONS in SH sample. Majority of the CHONS compounds have O/N ratio higher than 7 and only one sulfur atom (Figure S6). They are likely multifunctional organosulfates with an additional nitrate group present with the -ONO_2 group carrying three and the -OSO_3H group carrying four oxygen atoms, respectively.[16]

Part S3. Figures and Tables

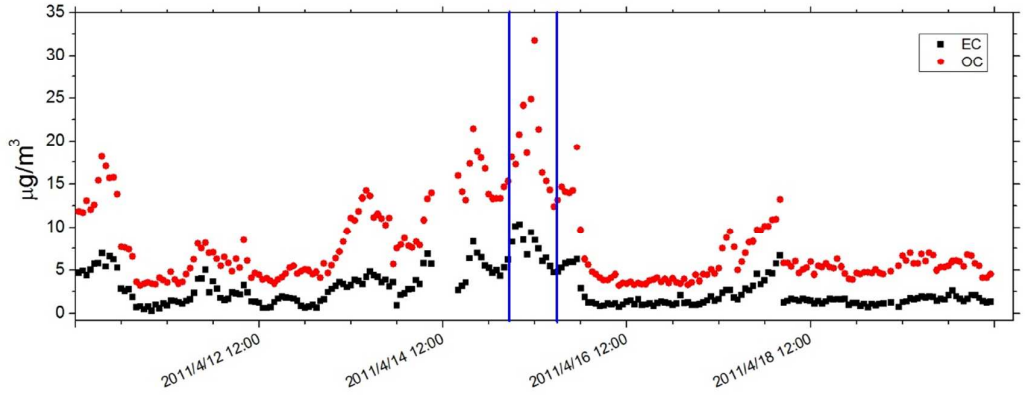

Figure S1. Time variation of the concentration of elemental carbon (EC) and organic carbon (OC) during April 10th – April 20th 2011, measured in the urban area of Shanghai. Two blue vertical lines show the sampling time for SH sample in this paper.

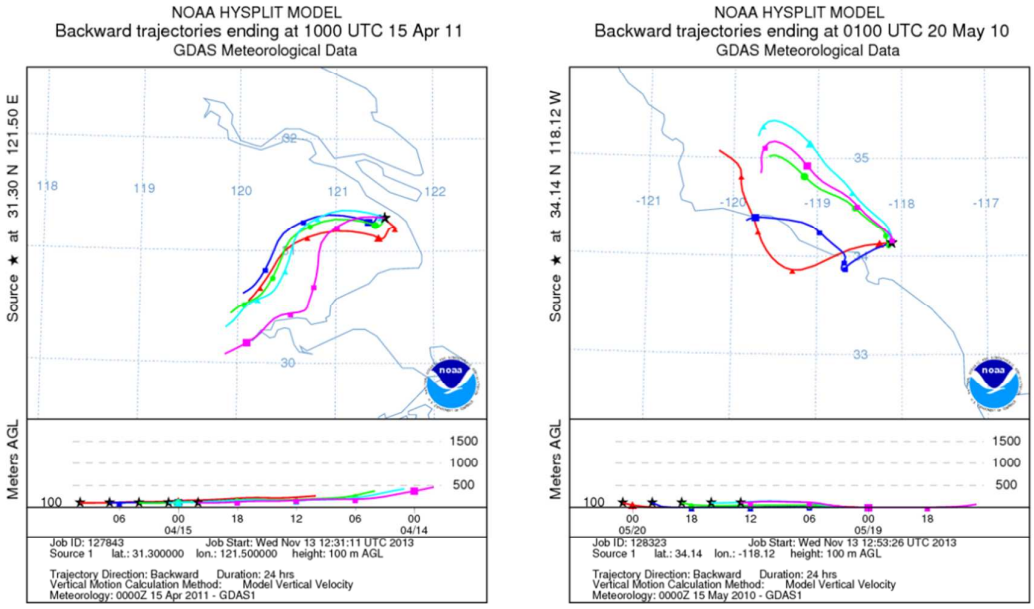

Figure S2. HYSPLIT trajectories for (left) SH sample and (right) LA sample.

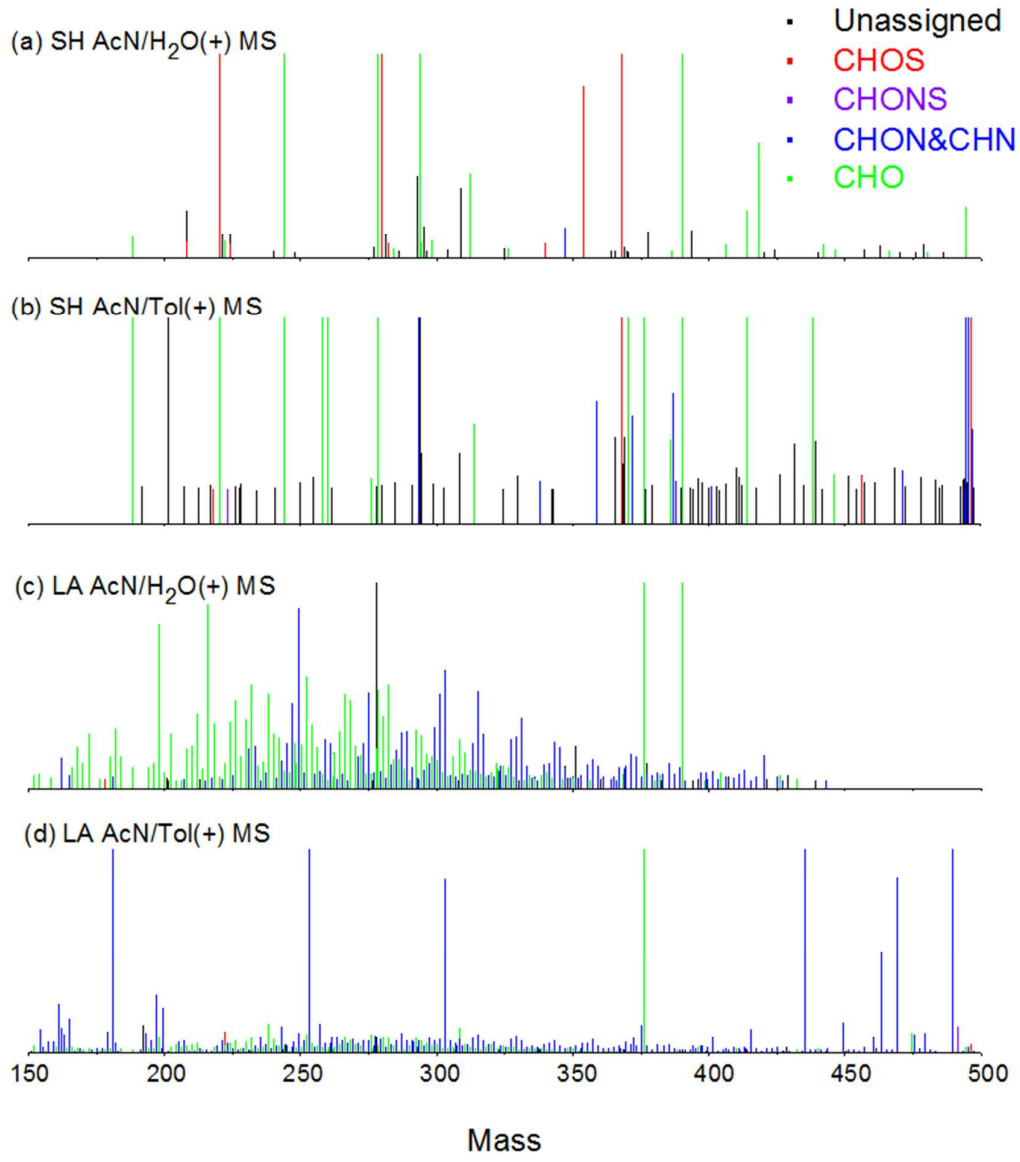

Figure S3. Nano-DESI HR-MS reconstructed mass spectra in positive mode. X-axis corresponds to the molecular weight of the neutral species. Different formula groups are marked in different colors. The unassigned peaks were converted into "neutral mass" on the assumption that they were protonated.

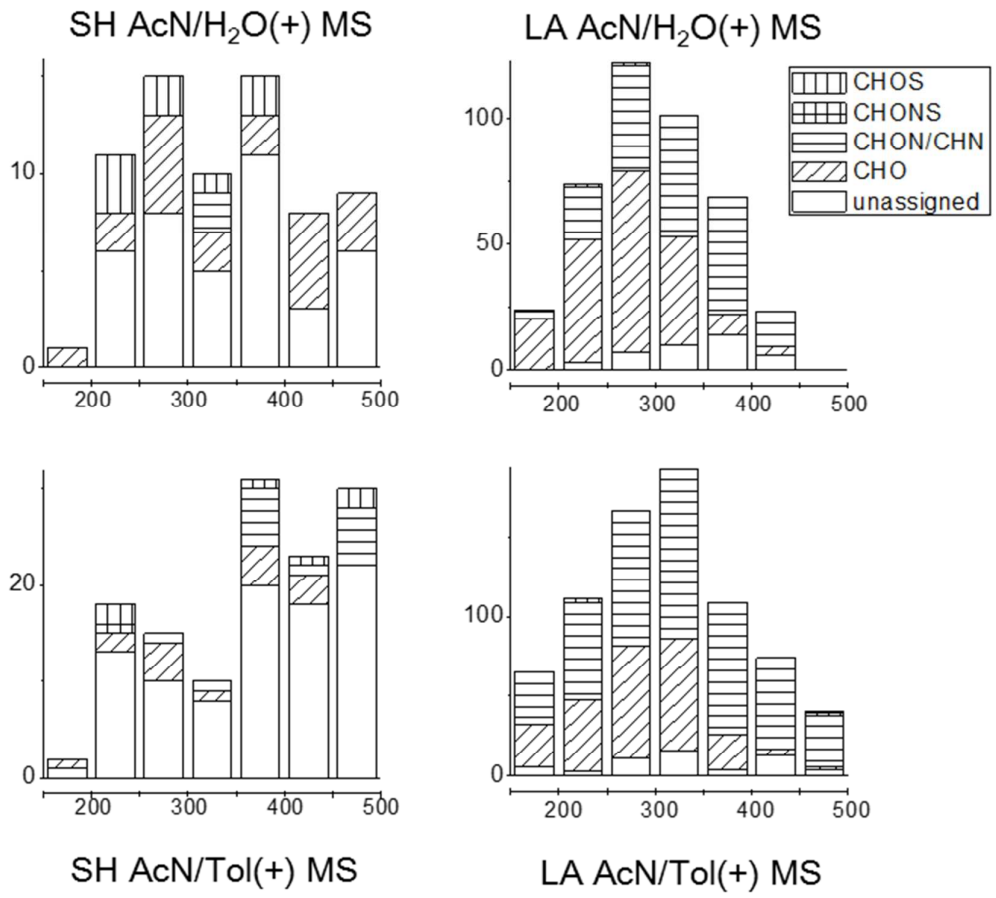

Figure S4. The number fraction of different species in the different mass ranges (positive mode). The bins are 50 Da wide.

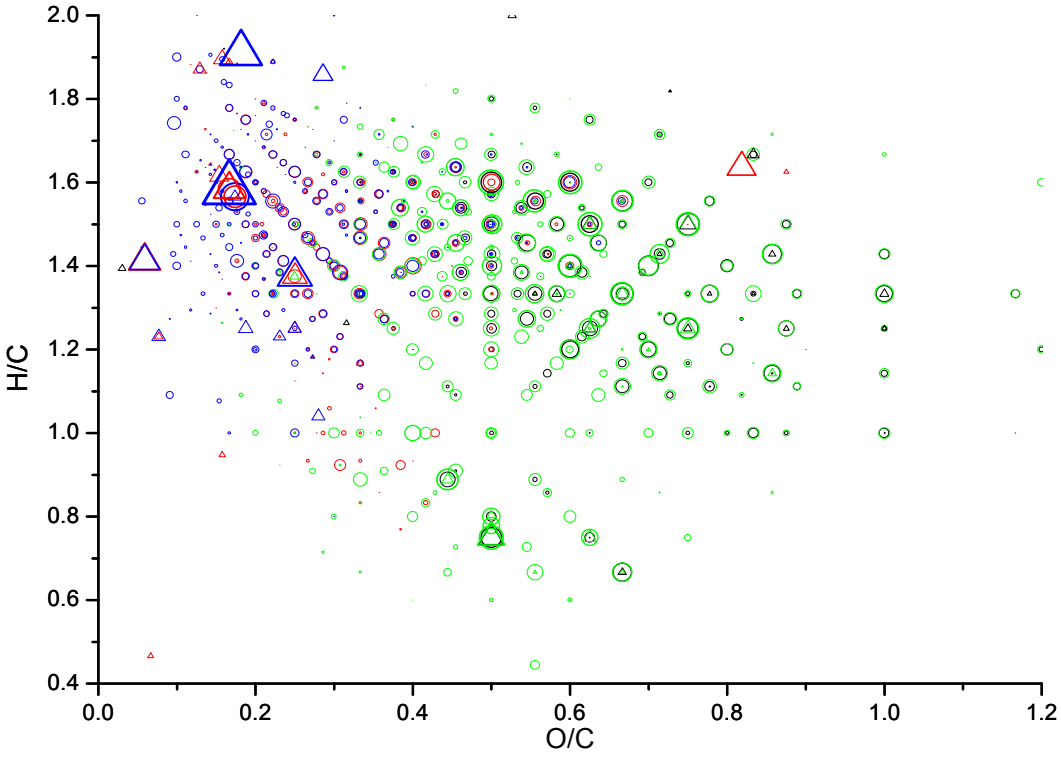

Figure S5. Van Krevelen diagrams for CHO species in (triangle)SH sample and (circle)LA sample. Red markers are compounds measured in AcN/H_2O(+) MS; black markers are compounds measured in AcN/H_2O(–) MS; blue markers are compounds measured in AcN/ Tol(+) MS; green markers are compounds measured in AcN/ Tol(–) MS. The size of the points is proportional to the logarithm of the corresponding peak intensity.

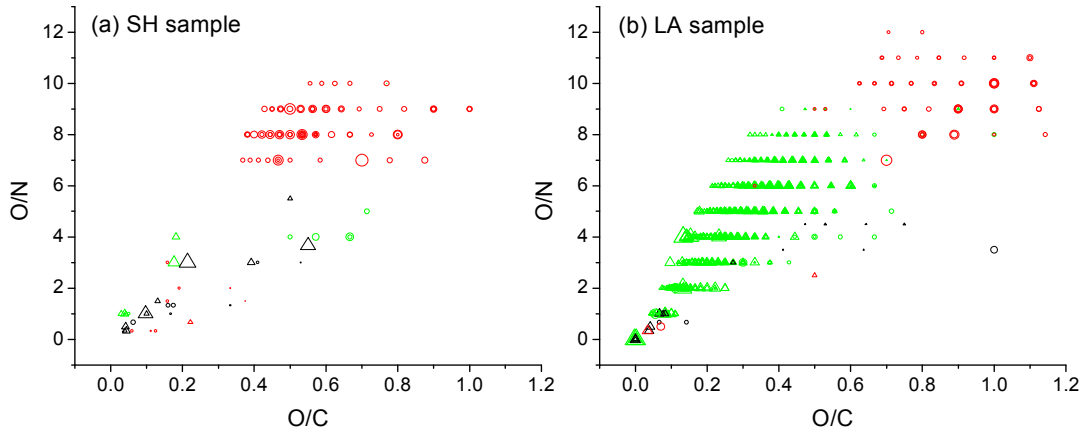

Figure S6. Van Krevelen diagrams by plotting O/N ratio against O/C ratio for N-OC species in (a) SH sample and (b) LA sample. Data plotted for CHONS are colored red; Data plotted by CHON/CHN containing only 1 N atom and CHON/CHN containing more than 1 N atoms are colored green and black respectively. Triangles represent compounds measured in positive mode while circles represent those measured in negative mode. The size of the points is proportional to the logarithm of the corresponding peak intensity.

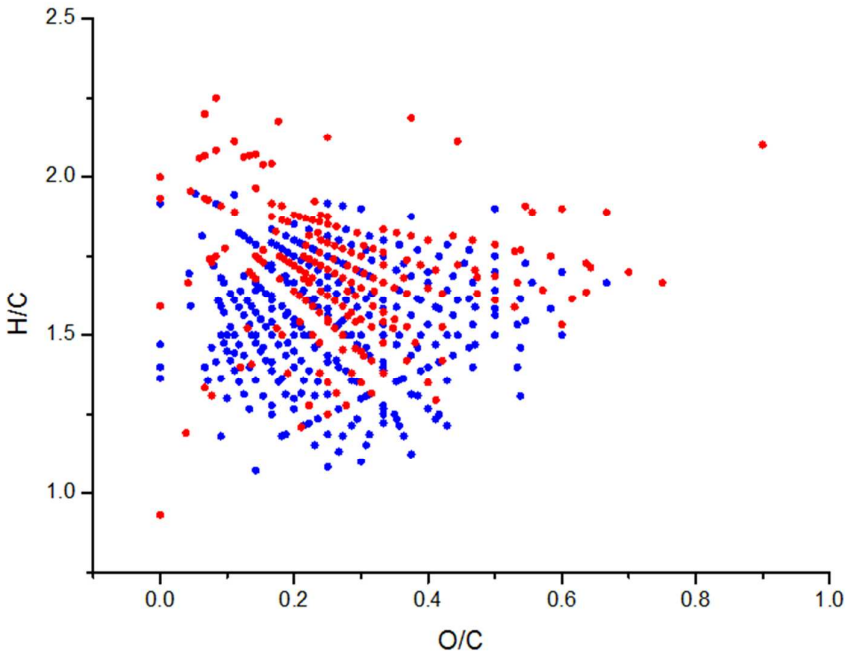

Figure S7. Van Krevelen diagram for the CHON and CHN compounds of LA sample observed in positive mode. The blue points correspond to compounds for which we observe a precursor with the mass differences given by immidization and subsequent cyclization and/or disproportionation. The red points correspond to compounds for which we do not observe a precursor.

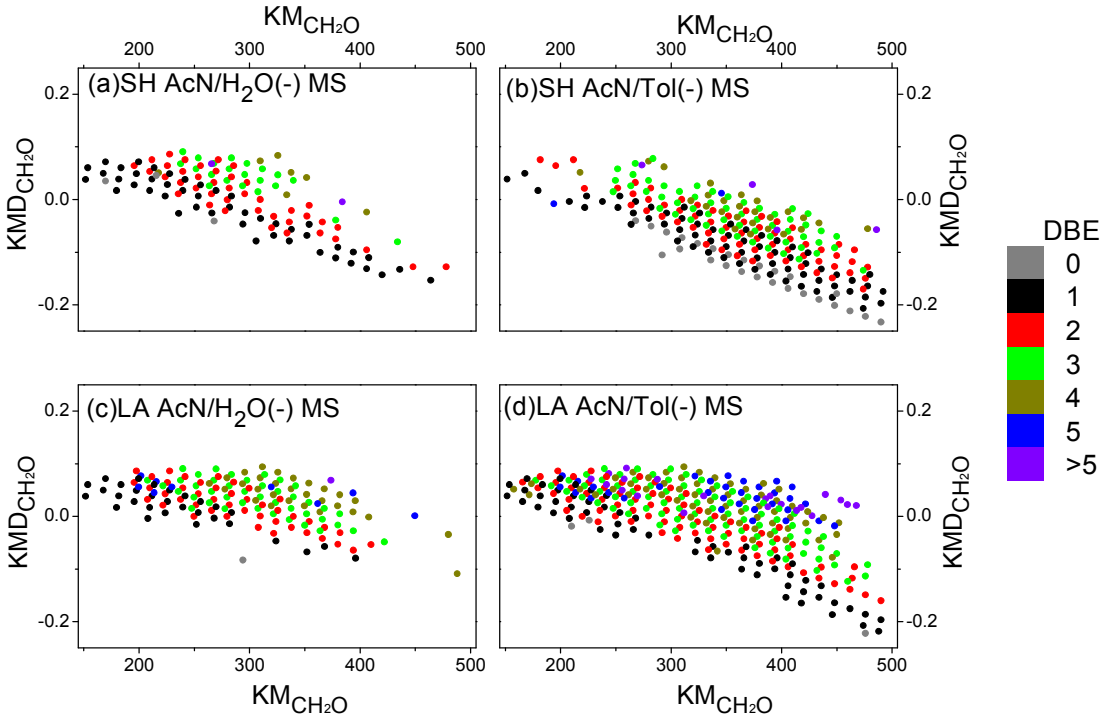

Figure S8. CH_2O-Kendrick diagrams for $CHOS_1$ detected in (a) SH AcN/H_2O(–) MS, (b) SH AcN/Tol(–) MS, (c) LA AcN/H_2O(–) MS and (d) LA AcN/Tol(–) MS. The color represents the DBE values calculated from Eq S1. Notice: the KMD_{CH2O} is calculated as Eq S3 if Nominal Mass–KM_{CH2O}<0.5, or KMD_{CH2O}=Nominal Mass–1–KM_{CH2O} if Nominal Mass–KM_{CH2O}>0.5, in order to avoid the break in the diagrams.

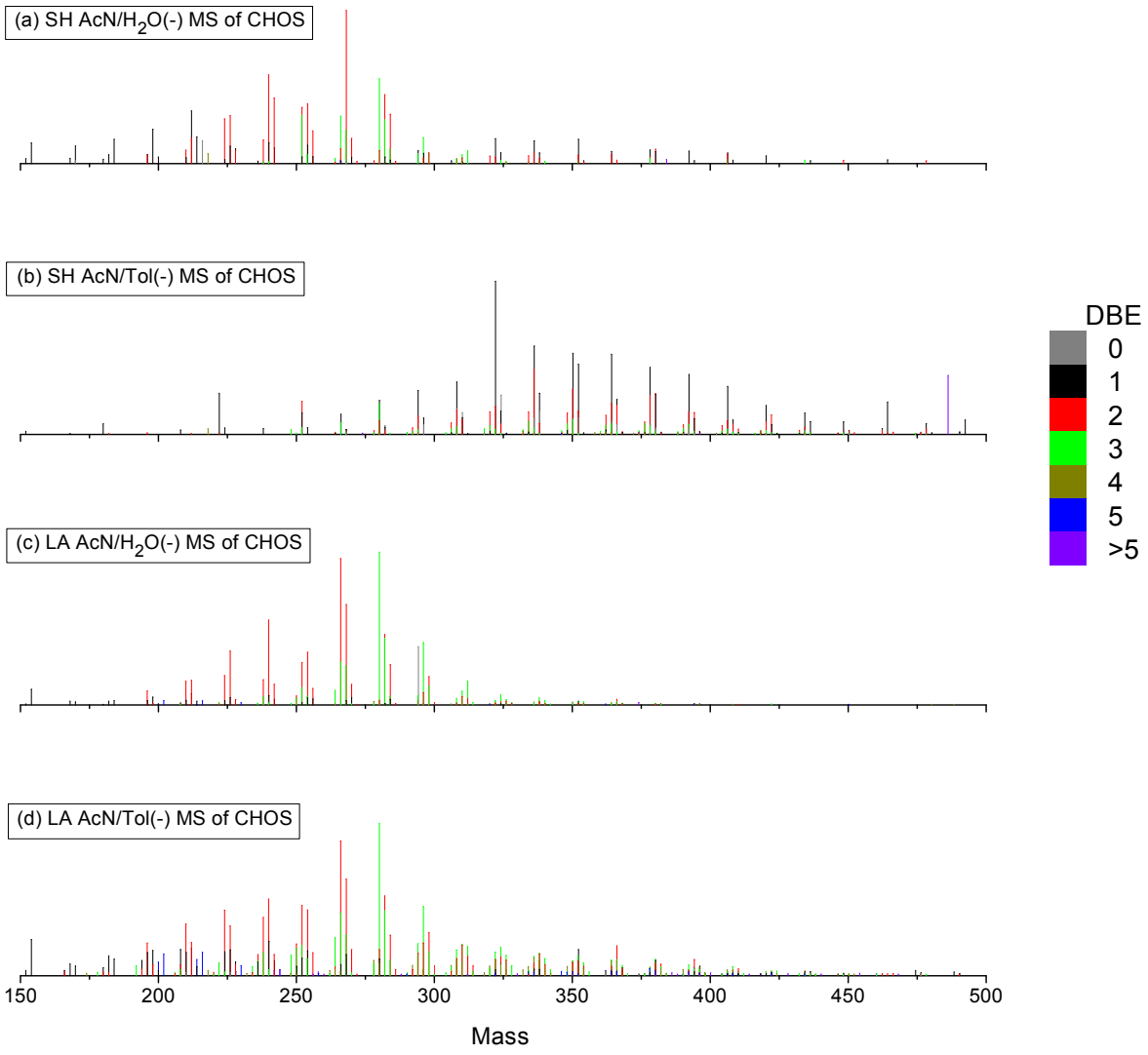

Figure S9. nano-DESI HR-MS reconstructed mass spectra of $CHOS_1$. X-axis corresponds to the molecular weight of the neutral species. Compounds with different DBE values calculated from Eq S1 are marked in different colors.

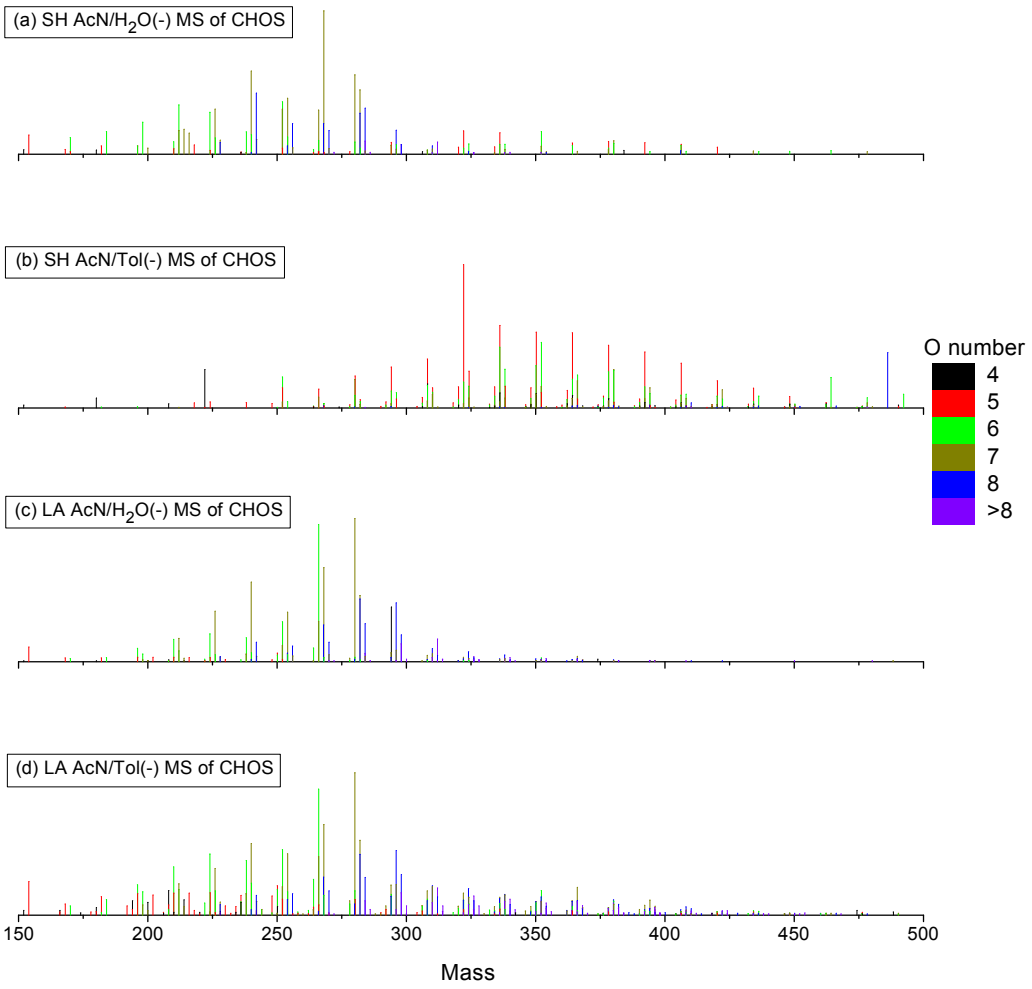

Figure S10. nano-DESI HR-MS reconstructed mass spectra of $CHOS_1$. X-axis corresponds to the molecular weight of the neutral species. Compounds containing different O number are marked in different colors.

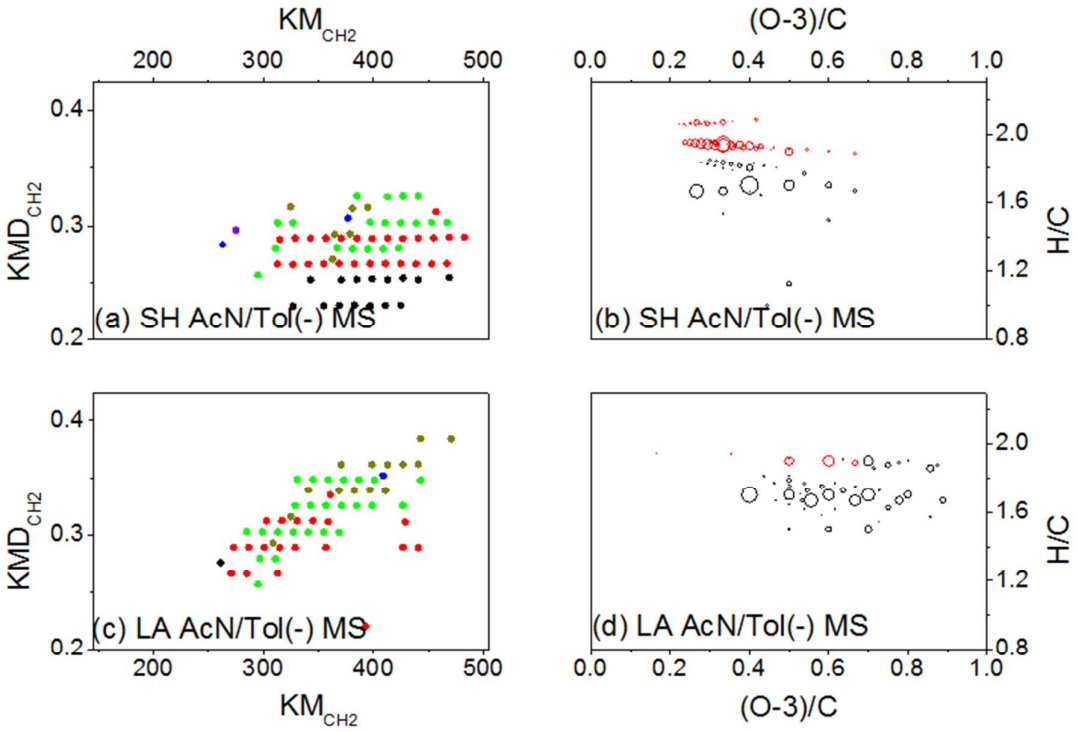

Figure S11. (a & c) CH_2-Kendrick diagrams and (b & d) Van Krevelen diagrams for the $CHONS_1$ in SH AcN/ Tol(–) MS and LA AcN/ Tol(–) MS. In CH_2-Kendrick diagrams, compounds with different DBE values calculated from Eq S1 are marked in different colors, by using the same color-code as that in Figure 1. In Van Krevelen diagrams, the size of the points is proportional to the logarithm of the corresponding peak intensity, and subgroup B CHONS are red-colored.

Table S1. The most abundant CHOS compounds and their intensities (in percent relative to the strongest peak in the mass spectrum). The peaks with relative intensity >10% in at least one spectrum are all listed here. The subgroup B CHOS are marked in red. The corresponding possible precursors are based on Ref. [15,16]. CHONS species were not listed and compared here due to their low occurrence.

Neutral Mass	Neutral Formula	Relative Intensity(%)				Approximate Precursor
		SH AcN/H_2O	SH AcN/Tol	LA AcN/H_2O	LA AcN/Tol	
182.0253	$C_5H_{10}O_5S$	5.8		2.6	13.1	Isoprene
196.0046	$C_5H_8O_6S$	5.7	1	9.3	21.5	Isoprene
196.0411	$C_6H_{12}O_5S$	5.9		3	15	
198.0203	$C_5H_{10}O_6S$	22.2		5.2	16.5	Isoprene
201.9941	$C_7H_6O_5S$			3	14.2	
208.0775	$C_8H_{16}O_4S$		2.9	1.4	17.2	
210.0203	$C_6H_{10}O_6S$	8.6		15.6	34	
210.0567	$C_7H_{14}O_5S$	3.7		3.2	15.5	
212.036	$C_6H_{12}O_6S$	34.4		7.4	18.1	
216.0096	$C_8H_8O_5S$			2.8	15.4	
222.0932	$C_9H_{18}O_4S$		26.9			
224.036	$C_7H_{12}O_6S$	29.2		19.3	43	monoterpene
224.0722	$C_8H_{16}O_5S$	2.5	4.3	2.9	15.7	
226.0152	$C_6H_{10}O_7S$	31.4		35.3	32.7	isoprene
226.0516	$C_7H_{14}O_6S$	11.3		5	17.1	
236.0721	$C_9H_{16}O_5S$	1.6			13.8	
238.0153	$C_7H_{10}O_7S$	1.2		5.3	15.2	isoprene
238.0515	$C_8H_{14}O_6S$	15.4		16.6	38.4	monoterpene
240.0308	$C_7H_{12}O_7S$	57.9		55.5	50.5	monoterpene
240.0671	$C_8H_{16}O_6S$	13.6		6.3	22.5	
248.0722	$C_{10}H_{16}O_5S$		3.2	1.2	13.6	monoterpene
250.0516	$C_9H_{14}O_6S$		0.5	4.6	18.1	monoterpene
250.0879	$C_{10}H_{18}O_5S$			5.9	20.9	monoterpene
252.0308	$C_8H_{12}O_7S$	31.5	4.3	11.3	20.1	
252.0672	$C_9H_{16}O_6S$	36.5	21.6	27.8	46.1	monoterpene; sesquiterpene
252.1037	$C_{10}H_{20}O_5S$	4.3	14	1.4	11.4	
254.0464	$C_8H_{14}O_7S$	39.1		34.5	43.2	monoterpene
254.0826	$C_9H_{18}O_6S$	12	4.4	4.9	16.4	

256.0257	$C_7H_{12}O_8S$	21.4		10.8	15.2	isoprene
264.0671	$C_{10}H_{16}O_6S$	3.4	1.5	9.7	25.1	monoterpene
266.0464	$C_9H_{14}O_7S$	30.9	7.6	28.1	41.1	
266.0828	$C_{10}H_{18}O_6S$	9.6	7.6	95.7	88.6	monoterpene
266.1185	$C_{11}H_{22}O_5S$	1.6	13.3		7.3	
268.0256	$C_8H_{12}O_8S$	21.5	1.7	25.7	26.8	isoprene
268.062	$C_9H_{16}O_7S$	100	3.3	65.6	63.6	monoterpene
268.0981	$C_{10}H_{20}O_6S$		3.2	2.8	13.9	
270.0413	$C_8H_{14}O_8S$	16.4		13.5	17.2	isoprene
280.062	$C_{10}H_{16}O_7S$	55.3	20	100	100	monoterpene
280.0983	$C_{11}H_{20}O_6S$	8.4	8.8	3.1	17.1	
280.1341	$C_{12}H_{24}O_5S$		22.2		11	
282.0412	$C_9H_{14}O_8S$	28.5		43.6	42.7	isoprene
282.0777	$C_{10}H_{18}O_7S$	44.9	2.5	46.1	52.5	monoterpene
284.0568	$C_9H_{16}O_8S$	32.1		26.5	26.6	monoterpene
294.0413	$C_{10}H_{14}O_8S$		0.9	2.8	13.2	
294.0777	$C_{11}H_{18}O_7S$	6.3	3	6.1	21.1	
294.1137	$C_{12}H_{22}O_6S$		11.8		14.6	
294.1504	$C_{13}H_{26}O_5S$	8.2	28.7			
294.1864	$C_{14}H_{30}O_4S$			38.2		
296.0568	$C_{10}H_{16}O_8S$	16.7		40.9	45.5	
296.0931	$C_{11}H_{20}O_7S$	3.5		7.9	21.6	
298.0361	$C_9H_{14}O_9S$	6.8		12.4	15.8	isoprene
298.0725	$C_{10}H_{18}O_8S$	6.7		18.6	28.6	monoterpene
308.0932	$C_{12}H_{20}O_7S$	3	5	4.5	17.1	
308.1296	$C_{13}H_{24}O_6S$	3	15.9	0.8	11.3	
308.1658	$C_{14}H_{28}O_5S$		34.2			
308.2025	$C_{15}H_{32}O_4S$		16.7			
310.0725	$C_{11}H_{18}O_8S$	5.7		9.2	20.7	
310.1085	$C_{12}H_{22}O_7S$	3.7	9.6	5.6	20	
310.1454	$C_{13}H_{26}O_6S$	1	11			
310.1817	$C_{14}H_{30}O_5S$		14.2			
312.0516	$C_{10}H_{16}O_9S$	8.4		15.8	19.3	
312.0879	$C_{11}H_{20}O_8S$			4.2	13	
320.1666	$C_{15}H_{28}O_5S$	4.8	14.7			
322.1088	$C_{13}H_{22}O_7S$		3.3	3	15.6	
322.1456	$C_{14}H_{26}O_6S$	4.3	18.1	0.9	10.7	
322.1812	$C_{15}H_{30}O_5S$	16.3	100		3.8	
324.088	$C_{12}H_{20}O_8S$	1.9	0.5	6.9	18.8	

324.1242	$C_{13}H_{24}O_7S$		6.9	2.3	12.5	
324.1607	$C_{14}H_{28}O_6S$	7	15.3	0.9	8	
324.1975	$C_{15}H_{32}O_5S$		25.6			
326.0672	$C_{11}H_{18}O_9S$	1.2		3.5	13.6	
334.1809	$C_{16}H_{30}O_5S$	5	14.7		1	
336.0886	$C_{13}H_{20}O_8S$		0.7	1.9	11.8	
336.1245	$C_{14}H_{24}O_7S$		4.1	1.5	12.7	
336.1608	$C_{15}H_{28}O_6S$	7	42.4		8.2	
336.1971	$C_{16}H_{32}O_5S$	14.9	57.6		4.4	
338.1035	$C_{13}H_{22}O_8S$		0.5	4.7	14.7	
338.1399	$C_{14}H_{26}O_7S$	3.2	7	2	14.3	
338.1765	$C_{15}H_{30}O_6S$	6.9	27		4.1	
338.2129	$C_{16}H_{34}O_5S$		15.1			
340.0829	$C_{12}H_{20}O_9S$	1.3		2.9	11.3	
348.1972	$C_{17}H_{32}O_5S$		14			
350.1767	$C_{16}H_{30}O_6S$		29.5		8.5	
350.2127	$C_{17}H_{34}O_5S$		52.9			
352.1192	$C_{14}H_{24}O_8S$		0.6	1.8	13	sesquiterpene
352.1551	$C_{15}H_{28}O_7S$	5.5	14.9	1	9.4	
352.1918	$C_{16}H_{32}O_6S$	15.9	45.8	2.7	17.3	
362.2128	$C_{18}H_{34}O_5S$		12.4			
364.1923	$C_{17}H_{32}O_6S$	6	20.2		6.2	
364.2287	$C_{18}H_{36}O_5S$	7.9	52.3		2.8	
366.1711	$C_{16}H_{30}O_7S$	2.1	19.1	3.6	19.6	
366.208	$C_{17}H_{34}O_6S$		23.1		3.2	
378.2079	$C_{18}H_{34}O_6S$	4.2	25.3		5.6	
378.2446	$C_{19}H_{38}O_5S$	8.8	43.8		2.2	
380.1869	$C_{17}H_{32}O_7S$	9.4	26.7	0.5	7.7	
380.2234	$C_{18}H_{36}O_6S$	7.7	26.1		10	
392.2235	$C_{19}H_{36}O_6S$		14.7		3.3	
392.2594	$C_{20}H_{40}O_5S$	8.1	39.1			
394.2028	$C_{18}H_{34}O_7S$		14.2	1	10.6	
406.2754	$C_{21}H_{42}O_5S$	6.9	31.2		1.2	
420.2912	$C_{22}H_{44}O_5S$	4.9	18.9		1.5	
422.2339	$C_{20}H_{38}O_7S$		12.7			
434.3068	$C_{23}H_{46}O_5S$		14		2.3	
464.3166	$C_{24}H_{48}O_6S$	2.3	21.2			
486.2284	$C_{24}H_{38}O_8S$		38.6			

References

(1)Ryerson, T. B.; Andrews, A. E.; Angevine, W. M.; Bates, T. S.; Brock, C. A.; Cairns, B.; Cohen, R. C.; Cooper, O. R.; de Gouw, J. A.; Fehsenfeld, F. C.; Ferrare, R. A.; Fischer, M. L.; Flagan, R. C.; Goldstein, A. H.; Hair, J. W.; Hardesty, R. M.; Hostetler, C. A.; Jimenez, J. L.; Langford, A. O.; McCauley, E.; McKeen, S. A.; Molina, L. T.; Nenes, A.; Oltmans, S. J.; Parrish, D. D.; Pederson, J. R.; Pierce, R. B.; Prather, K.; Quinn, P. K.; Seinfeld, J. H.; Senff, C. J.; Sorooshian, A.; Stutz, J.; Surratt, J. D.; Trainer, M.; Volkamer, R.; Williams, E. J.; Wofsy, S. C., The 2010 California Research at the Nexus of Air Quality and Climate Change (CalNex) field study. *J. Geophys. Res.* **2013,** *118*, (11), 5830-5866.

(2)Hayes, P. L.; Ortega, A. M.; Cubison, M. J.; Froyd, K. D.; Zhao, Y.; Cliff, S. S.; Hu, W. W.; Toohey, D. W.; Flynn, J. H.; Lefer, B. L.; Grossberg, N.; Alvarez, S.; Rappenglueck, B.; Taylor, J. W.; Allan, J. D.; Holloway, J. S.; Gilman, J. B.; Kuster, W. C.; De Gouw, J. A.; Massoli, P.; Zhang, X.; Liu, J.; Weber, R. J.; Corrigan, A. L.; Russell, L. M.; Isaacman, G.; Worton, D. R.; Kreisberg, N. M.; Goldstein, A. H.; Thalman, R.; Waxman, E. M.; Volkamer, R.; Lin, Y. H.; Surratt, J. D.; Kleindienst, T. E.; Offenberg, J. H.; Dusanter, S.; Griffith, S.; Stevens, P. S.; Brioude, J.; Angevine, W. M.; Jimenez, J. L., Organic aerosol composition and sources in Pasadena, California, during the 2010 CalNex campaign. *J. Geophys. Res.* **2013,** *118*, (16), 9233-9257.

(3)Roach, P. J.; Laskin, J.; Laskin, A., Molecular Characterization of Organic Aerosols Using Nanospray-Desorption/Electrospray Ionization-Mass Spectrometry. *Anal. Chem.* **2010,** *82*, (19), 7979-7986.

(4)Roach, P. J.; Laskin, J.; Laskin, A., Nanospray desorption electrospray ionization: an ambient method for liquid-extraction surface sampling in mass spectrometry. *Analyst* **2010,** *135*, (9), 2233-2236.

(5)Roach, P. J.; Laskin, J.; Laskin, A., Higher-Order Mass Defect Analysis for Mass Spectra of Complex Organic Mixtures. *Anal. Chem.* **2011,** *83*, (12), 4924-4929.

(6)Wozniak, A. S.; Bauer, J. E.; Sleighter, R. L.; Dickhut, R. M.; Hatcher, P. G., Technical Note: Molecular characterization of aerosol-derived water soluble organic carbon using ultrahigh resolution electrospray ionization Fourier transform ion cyclotron resonance mass spectrometry. *Atmos. Chem. Phys.* **2008,** *8*, (17), 5099-5111.

(7)Fuller, S. J.; Zhao, Y. J.; Cliff, S. S.; Wexler, A. S.; Kalberer, M., Direct Surface Analysis of Time-Resolved Aerosol Impactor Samples with Ultrahigh-Resolution Mass Spectrometry. *Anal. Chem.* **2012,** *84*, (22), 9858-9864.

(8)KENDRICK, E., A MASS SCALE BASED ON CH2=14.0000 FOR HIGH RESOLUTION MASS SPECTROMETRY OF ORGANIC COMPOUNDS. *Anal. Chem.* **1963,** *35*, (13), 2146-&.

(9)Kim, S.; Kramer, R. W.; Hatcher, P. G., Graphical method for analysis of ultrahigh-resolution broadband mass spectra of natural organic matter, the van Krevelen diagram. *Anal. Chem.* **2003,** *75*, (20), 5336-5344.

(10)Laskin, J.; Laskin, A.; Roach, P. J.; Slysz, G. W.; Anderson, G. A.; Nizkorodov, S. A.; Bones, D. L.; Nguyen, L. Q., High-Resolution Desorption Electrospray Ionization Mass Spectrometry for Chemical Characterization of Organic Aerosols. *Anal. Chem.* **2010,** *82*, (5), 2048-2058.

(11)O'Brien, R. E.; Laskin, A.; Laskin, J.; Liu, S.; Weber, R.; Russell, L. M.; Goldstein, A. H., Molecular characterization of organic aerosol using nanospray desorption/electrospray ionization mass spectrometry: CalNex 2010 field study. *Atmos. Environ.* **2013,** *68*, 265-272.

(12)Paulot, F.; Crounse, J. D.; Kjaergaard, H. G.; Kroll, J. H.; Seinfeld, J. H.; Wennberg, P. O., Isoprene photooxidation: new insights into the production of acids and organic nitrates. *Atmos. Chem. Phys.* **2009,** *9*, (4), 1479-1501.

(13)Darer, A. I.; Cole-Filipiak, N. C.; O'Connor, A. E.; Elrod, M. J., Formation and Stability of Atmospherically Relevant Isoprene-Derived Organosulfates and Organonitrates. *Environ. Sci. Technol.* **2011,** *45*, (5), 1895-1902.
(14)Hu, K. S.; Darer, A. I.; Elrod, M. J., Thermodynamics and kinetics of the hydrolysis of atmospherically relevant organonitrates and organosulfates. *Atmos. Chem. Phys.* **2011,** *11*, (16), 8307-8320.
(15)Chan, M. N.; Surratt, J. D.; Chan, A.; Schilling, K.; Offenberg, J. H.; Lewandowski, M.; Edney, E. O.; Kleindienst, T. E.; Jaoui, M.; Edgerton, E. S.; Tanner, R. L.; Shaw, S. L.; Zheng, M.; Knipping, E. M.; Seinfeld, J. H., Influence of aerosol acidity on the chemical composition of secondary organic aerosol from beta-caryophyllene. *Atmos. Chem. Phys.* **2011,** *11*, (4), 1735-1751.
(16)Surratt, J. D.; Gomez-Gonzalez, Y.; Chan, A.; Vermeylen, R.; Shahgholi, M.; Kleindienst, T. E.; Edney, E. O.; Offenberg, J. H.; Lewandowski, M.; Jaoui, M.; Maenhaut, W.; Claeys, M.; Flagan, R. C.; Seinfeld, J. H., Organosulfate formation in biogenic secondary organic aerosol. *J. Phys. Chem. A* **2008,** *112*, (36), 8345-8378.